ResearchGate

See discussions, stats, and author profiles for this publication at: https://www.researchgate.net/publication/276205560

Evolution of Kerogen and Bitumen during Thermal Maturation via Semi-Open Pyrolysis Investigated by Infrared Spectroscopy

ARTICLE *in* ENERGY & FUELS · APRIL 2015

Impact Factor: 2.79 · DOI: 10.1021/ef5027532

READS

60

7 AUTHORS, INCLUDING:

Paul R. Craddock

Schlumberger Limited

34 PUBLICATIONS **636** CITATIONS

SEE PROFILE

Alyssa M. Charsky

Colorado School of Mines

3 PUBLICATIONS **2** CITATIONS

SEE PROFILE

Andrew E Pomerantz

Schlumberger Limited

82 PUBLICATIONS **1,283** CITATIONS

SEE PROFILE

Available from: Andrew E Pomerantz

Retrieved on: 02 February 2016

energy&fuels

Article

pubs.acs.org/EF

Evolution of Kerogen and Bitumen during Thermal Maturation via Semi-Open Pyrolysis Investigated by Infrared Spectroscopy

Paul R. Craddock,* Tuong Van Le Doan, Kyle Bake, Marina Polyakov, Alyssa M. Charsky, and Andrew E. Pomerantz

Schlumberger-Doll Research, 1 Hampshire Street, Cambridge, Massachusetts 02139, United States

ABSTRACT: A series of artificial maturation (anhydrous, semi-open pyrolysis) experiments on Green River oil shale have been performed to simulate the thermal maturation of type I kerogen. The goals of this program were to develop a kinetic model of petroleum generation from oil shale and to characterize the yield and composition of petroleum as a function of artificial thermal maturity. The thermal maturity level (EASY%Ro = 0.48−1.28%) is based upon the kinetic model of kerogen degradation and is equivalent to vitrinite reflectance maturity. Here, we compare the structural characteristics of kerogen and bitumen during artificial maturation of oil shale using quantitative Fourier transform infrared (IR) spectroscopy. Quantitative comparison was enabled by a novel method for the preparation of bitumen for IR spectroscopy. Bitumen can be a reaction intermediate during maturation of kerogen, and the IR data indicate that bitumen has a structure intermediate between that of kerogen and generated petroleum. Moreover, the IR data reveal that the composition of bitumen changes with maturity, with trends that are similar in some aspects to those observed previously in kerogen, but different in others. Kerogen is characterized by the early depletion of oxygenated functional groups prior to petroleum generation (EASY%Ro < 0.9%) and then a late enrichment of oxygen at higher artificial maturity (EASY%Ro > 1.2%). In contrast, bitumen shows initial enrichment of oxygenated functional groups at low artificial maturity (EASY%Ro < 0.8%) and subsequent depletion at higher maturity. Kerogen evolution follows the previously observed trend with aliphatic carbon chains that became shorter and/or more branched as kerogen is consumed during all stages of artificial maturation. Bitumen, in contrast, appears to have aliphatic carbon chains that lengthen within the same artificial maturity range as bitumen is predominantly generated from kerogen. The aliphatic carbon content of bitumen is greater than that of kerogen at all levels of artificial maturity. Both kerogen and bitumen become more aromatic in character with increasing thermal maturity, especially above artificial levels EASY%Ro > 0.9%. This similarity likely results from loss of aliphatic chains from both organic fractions during petroleum generation, suggesting that both kerogen and bitumen can be direct sources for petroleum. The loss of aliphatic carbons from aromatic centers in both kerogen and bitumen leads to protonation of the residual aromatic rings. The IR spectra of kerogen and bitumen indicate very similar degrees of protonation of those aromatic rings.

INTRODUCTION

Oil shale is sedimentary rock which contains immature organic matter that has not undergone thermal conversion to petroleum (oil and hydrocarbon gas). The production of petroleum from oil shale has long been undertaken by mining of near-surface deposits coupled to surface retorting. Methods of thermally maturing ("pyrolyzing") oil shale in situ have been explored as a means of generating hydrocarbons from these resources at economic scales.[1−8] In situ processing could offer a practical means for the thermal conversion of deeply buried oil shale.

Recently, we carried out a series of anhydrous, semi-open pyrolysis experiments using shale from the Garden Gulch Member of the Green River oil shale, Piceance Basin, Colorado.[8] The pyrolysis involved the heating of Green River oil shale samples at a range of temperatures (303 to 425 °C) and pressures (10 to 40 atm), and for a range of times between 5 and 12.5 h. This paper describes the characterization of a series of kerogen and bitumen samples isolated from the pyrolysis experiments and analyzed using quantitative Fourier transform infrared (IR) spectroscopy in an effort to compare the structural changes in these organic constituents as a function of simulated thermal maturity. Previously, IR spectroscopy techniques have been applied to the study of functional groups in coals and kerogen,[9−21] with particular attention paid to changes in structure of the carbon skeleton as a function of rank or thermal maturity. These studies generally indicate an increase in aromatic carbon content of coal and kerogen during thermal maturation, together with loss of heteroatom functional groups and a decrease in aliphatic carbon content. Studies of kerogen specific to the Green River Formation have documented the same gross structural changes with increasing degree of thermal maturation.[22]

Both kerogen (defined here as organic matter that is nonvolatile under pyrolysis conditions and insoluble in organic solvents) and bitumen (nonvolatile under pyrolysis conditions and soluble in organic solvents) can be present in source rocks and may impact the flow of petroleum through the low-permeability pore network in these formations. Bitumen can be an intermediate in the generation of petroleum from kerogen, as well as having a chemical structure and molecular weight that are intermediate between that of kerogen and petroleum.[23] Despite the potential importance of bitumen in petroleum generation and flow, its structure has received considerably less

Received: December 8, 2014
Revised: February 21, 2015
Published: February 26, 2015

ACS Publications © 2015 American Chemical Society

DOI: 10.1021/ef5027532
Energy Fuels 2015, 29, 2197−2210

study than has that of kerogen.[24,25] Here, we developed a novel method for the preparation of bitumen for quantitative IR spectroscopy so that a true comparison of the molecular-level structural evolution of bitumen and kerogen as a function of thermal maturity can be made. The IR spectroscopy results presented here provide unique insights to the comparable evolution of kerogen and bitumen and aid our understanding of the mechanisms by which oil and gas are produced in oil shale and other unconventional reservoirs.

EXPERIMENTAL SECTION

Green River Oil Shale. The oil shale sample and artificial maturation (pyrolysis) experiments on which this study is based are described in detail by Le Doan et al.[8] Briefly, Green River oil shale comprises fine-grained lacustrine sediments deposited in Lake Uinta across much of the Piceance and Uinta Basins between approximately 55 and 45 Ma.[26] The starting shale sample for the pyrolysis experiments was recovered in Rio Blanco County, Colorado (Piceance Basin) as cuttings from the Garden Gulch Member of the Green River Formation, at a depth between 2012 and 2088 ft within the illite-rich R-1 zone. The mineral composition of this Green River oil shale on a dry-weight basis as determined by Fourier transform infrared spectroscopy (FTIR) is illite (~35 wt %), quartz (20 wt %), dolomite plus calcite (18 wt %), buddingtonite [$(NH_4)AlSi_3O_8$] (13 wt %), and minor (<5 wt %) potassium feldspar, other clays, and pyrite. The shale is rich in organic matter, which is predominantly type I kerogen together with a little native bitumen. The total organic carbon (TOC) content of the immature shale prior to pyrolysis was approximately 14 wt %.

The cuttings were recovered by reverse circulation drilling in water. Room-dried cuttings were used as received. Cuttings were homogenized, split, and crushed to less than 100 μm as described by Le Doan et al.[8] The starting composition of the oil shale used for each pyrolysis experiment (defined as "native state" oil shale) was identical as confirmed by geochemical and mineralogical analyses.[8]

Pyrolysis Products. A complete description of the experimental setup and operating conditions for the pyrolysis runs is given in Le Doan et al.[8] Briefly, 93.2 g fractions of homogenized native state shale were thermally matured at a specified temperature and pressure (303–425 °C; 10–40 atm) under semi-open conditions for a range of durations from 5 to 12.5 h. The semi-open reactor enabled produced volatile components to escape the pyrolysis chamber while maintaining isobaric conditions. The resulting pyrolysis products and residual kerogens, therefore, have a range of thermal histories and maturities. The thermal maturity of organic matter following the pyrolysis experiment was computed as a synthetic vitrinite reflectance from the established "EASY%Ro" relationship published by Sweeney and Burnham.[27,28] The EASY%Ro is a comparable analog to the well-known vitrinite reflectance, Ro, estimate of organic thermal maturity and can be used in organic-bearing samples in which vitrinite macerals are absent. Thermal maturation of kerogen in the native state shale led to the production of bitumen, oil, and hydrocarbon gases, as well as inorganic species including water, CO_2, and H_2S (Figure 1). Kerogen in this study comprises both pyrolyzable carbon that has the potential to generate additional petroleum as well as the inert carbon residuum (commonly referred to as char or coke) that has no petroleum-generation potential. Bitumen here is defined as the organic fraction that is nonvolatile under pyrolysis conditions (i.e., retained in the pyrolysis chamber) but soluble and extractable in conventional organic solvents. Oil and hydrocarbon gas are the lower-molecular-weight organic fractions that are volatile under pyrolysis conditions. Oil and all gases escaped the reactor at pyrolysis conditions in the gas phase via pressure-controlled valves, which maintained the pressure in the reactor at the specified conditions. Oil was subsequently separated from gas by condensation from the evolved pyrolysis gases at standard temperature and pressure (25 °C, 1 atm). Water was commonly condensed along with the oil, removed by centrifugation, and studied separately. Methods for their recovery are described in full by Le Doan et al.[8]

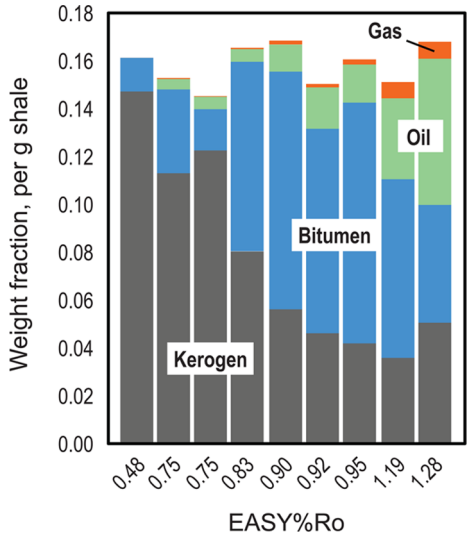

Figure 1. Distribution of organic fractions in Green River oil shale during thermal maturation (pyrolysis). The initial mass of organic fractions in the native state shale (EASY%Ro = 0.48%) is ~16 wt %. Pyrolyzed spent shales show near mass-closure with respect to organic components. Kerogen is represented as the sum of pyrolyzable and residual organic matter as determined by Rock-Eval. Kerogen is defined by the fraction of organics that is nonvolatile at pyrolysis conditions and insoluble in organic solvents. Kerogen comprises both pyrolyzable carbon as well as inert carbon that has no petroleum-generation potential. Bitumen is defined by the fraction of organics that is nonvolatile at pyrolysis conditions but soluble in organic solvents.

Kerogen and bitumen were retained in the bulk sample after pyrolysis (defined as "spent shale"). Bitumen was isolated from the spent shale using Soxhlet extraction by dissolution in a solvent mixture of dichloromethane and methanol, 9:1 ratio by volume. Extractions typically ran for 72–96 h. Bitumen was subsequently recovered from solution by rotary evaporation of the solvent mixture at temperatures <100 °C. This bitumen should be representative of the initial bulk because bitumen is nonvolatile at pyrolysis temperatures (>303 °C). Kerogen was isolated by demineralization of the inorganic matrix in the extracted spent shale. Inorganic minerals were dissolved by sequential acid treatment[29] using excess 3 N HCl, 3 N HCl + 14 N HF, and 14 N HF + 3% w/w boric acid [$B(OH)_3$], which was developed for the isolation of type I kerogen from Green River oil shale. The acid treatment for each step proceeded at ~80 °C for a period up to 24 h. Between each acid treatment, the residual solids were washed thoroughly with high-purity water. Boric acid was used in the final acid treatment to remove neoformed fluorosilicates. Pyrite is the principal mineral that cannot be effectively demineralized by this acid treatment procedure.[29] The presence of pyrite in the kerogen concentrate affects the absolute geochemical composition of the bulk concentrate. However, and most importantly, the presence of pyrite does not affect the measured IR spectrum of kerogen because the IR absorbance bands of pyrite are small and do not overlap with those in the spectra of organic materials. A second solvent extraction procedure was used on the isolated kerogen to remove residual bitumen not previously recovered from the spent shale. The second bitumen extract comprised between 4 and 8% of the total bitumen, indicating that the primary extraction of the bulk shale was effective. The isolated bitumen and kerogen fractions were retained for subsequent geochemical and spectroscopic study.

Geochemical Measurements. X-ray fluorescence (XRF) measurements of the kerogen isolate were made in loose powder form to confirm the absence of inorganic minerals. The measurements were made using a Spectro XeposHE energy-dispersive XRF instrument

DOI: 10.1021/ef5027532
Energy Fuels 2015, 29, 2197–2210

using the factory configuration. The data are considered semi-quantitative for kerogen because the method is not optimized for organic-rich matrices.

Determination of the C and H content of the kerogen and bitumen isolates was made using routine combustion methods with a PerkinElmer CHN analyzer. The kerogen compositions are reported by the atomic H/C ratio because this ratio is not affected in any way by the presence of residual pyrite in the kerogen concentrate. The C and H composition of bitumen is similarly reported at the atomic H/C ratio for comparison with kerogen compositions.

FTIR Spectroscopy: Sample Preparation and Spectral Collection. The principles of infrared spectroscopy for the analysis of solid and liquid samples are well-known. Transmission IR spectroscopy of solid-phase samples is subject to optical artifacts including Lorentz−Mie scattering (scattering of electromagnetic radiation by particles larger than the photon wavelength) and the Christiansen effect (influence of the refractive index contrast between a solid sample and suspending matrix on the transmission of electromagnetic radiation).[30] Quantitative interpretation of transmission IR spectra (i.e., comparison of absolute peak amplitudes) requires that samples obey the Beer−Lambert law, which states that the total absorption of light by an attenuating substance, expressed as $-\log_{10}(I/I_0)$, is linearly proportional to the concentration and molar absorptivity of the attenuator:

$$A = \log_{10}(1/T) = -\log_{10}(I/I_0) = \varepsilon l c \quad (1)$$

where ε is the absorptivity at the appropriate IR frequency (also referred to as extinction coefficient), l the path length of the IR beam (sample thickness), and c the concentration of the sample or attenuating substance in the sample. Where this relation holds, absorbance is a linear function of the concentration of material components in the matrix. The optical artifacts and requirements for quantitative IR spectroscopy require appropriate sample preparation.

Kerogen. The potassium bromide (KBr) pellet method is the most common for acquiring IR spectra of solids such as kerogen, in which the absorbing solid is finely ground and homogeneously dispersed in the powdered halide matrix.[10,11,29] Kerogen samples were first hand ground in an organic-clean mortar, and a precisely known quantity of ground kerogen (nominally 1.000 ± 0.010 mg) was added to a 5 mL volume mixing vial. The mixing vial is clean tungsten carbide containing two 7 mm diameter agate spheres. The KBr was received as a fine powder (XL Spectrograde, International Crystal Laboratories, Garfield, NJ). The KBr powder was treated by heating overnight (16 h) at 450 °C in air to remove any organic impurities that may otherwise compromise the IR organic signal. Then, 900.00 ± 0.50 mg of prepared KBr powder was weighed out. The kerogen and KBr were mixed incrementally to provide effective grinding and homogeneous distribution of kerogen in the KBr matrix.[29] In the incremental mixing process, a mass fraction of the KBr equivalent to the mass of kerogen was added to the mixing vial. The two components were mixed in an automixer (Retsch MM400, Verder Scientific Inc., Newtown, PA) for 5 min at 23 Hz. Subsequent addition of KBr to the mixture was made by adding a mass fraction of KBr equivalent to the total mass of the mixture in the vial. In total, six additions were made for a total mixing time of 30 min. The use of KBr not only reduced light scattering but also enabled a quantitative analysis of IR peak intensities because the sample mass and ratio in the KBr matrix was precisely controlled. Homogenous powder mixtures were next pressed into pellets of consistent size; 200.00 ± 0.50 mg of the powdered mixture was placed into a prepared die and then pressed into a clear pellet at 10 tons/cm^2 for 10 min under vacuum. The sample was then ready for IR analysis. We have found that mixing kerogen and KBr together in bulk (i.e., a single mix) did not yield a homogeneous mixture either in the powder or the subsequent pellet.

Bitumen. Organic phases that are liquid or soluble in organic solvents, such as bitumen and asphaltene, are commonly prepared in liquid or solution form. One method for analysis is to deposit the liquid or solution on a leveled surface of KBr powder or pellet and to evaporate any solvent, leaving the analyte in solid form on the KBr matrix.[14,31,32] A second method for analysis is to trap a thin film of the liquid or solution between two salt (e.g., NaCl, KBr) plates.[33] In both approaches, the thickness of the sample (i.e., l in eq 1) is unknown, can be heterogeneous, and/or is not readily controlled between samples, such that it is difficult to interpret the spectra in a quantitative manner.[33] In particular, the absolute peak intensities are difficult to interpret when the concentration and thickness of the sample are poorly controlled. Moreover, organic solvents required to dissolve bitumen or similar organic materials may have IR absorption characteristics that interfere with those of the analyte of interest when not removed in the salt-plate method, commonly limiting the interpretation of the IR characteristics of the analyte to a fraction of the available IR spectrum.

A means to overcome these limitations is to prepare bitumen as a solid, with sufficiently small particle size and homogeneously distributed within a KBr pellet as is done for the preparation of kerogen and coals. This enables the bitumen IR spectra to be interpreted both relatively and absolutely, and without spectral interference. For this study, bitumen samples were prepared for IR analysis in our laboratory using a novel cryomill method. This method used cryogenic temperatures at approximately −196 °C to embrittle the bitumen (i.e., temperatures below the glass-transition temperature of bitumen) that was otherwise ductile and did not grind or mix effectively in KBr at ambient temperature. The method used 900.00 ± 0.50 mg of prepared KBr powder, as described above. The KBr was added in full to a 5 mL volume cryomill vial that contained eight 5 mm zirconium oxide (ZrO_2) mixing spheres. A precisely known mass of dry bitumen (between 20 and 30 mg) was dissolved in a known volume of dichloromethane (DCM) solvent such that the concentration of bitumen in solution was recorded. A micropipette was used to transfer a known fraction of the DCM solution to the 5 mL volume cryomill vial so that the required mass of bitumen was obtained (nominally 1.00 mg). The DCM was allowed to evaporate completely by placing the cryomill vial on a hot plate at 40 °C. Once the DCM was evaporated, the vial was capped and placed inside a cryomill (Retsch CryoMill, Verder Scientific Inc.). The cryomill cycle was run with a 3 min cooling stage using liquid N_2, followed by a 15 min, 23 Hz mixing stage. The cryomill cycle was repeated once. The vial was removed from the cryomill and allowed to warm inside an oven set at 60 °C to drive off condensed vapors. The homogeneous mixture was removed from the cryomill vial, and a pellet was prepared from 200.00 ± 0.50 mg of the bitumen−KBr mixture using the identical method described for kerogen−KBr mixture. Only bitumen from the primary solvent extraction was studied in detail; the second bitumen extract comprised only a minor fraction (4 to 8%) of the total bitumen.

FTIR Spectral Analysis. The kerogen−KBr and bitumen−KBr pellets were scanned using a Bruker Vertex70 dual-range Fourier transform IR spectrometer. The Fourier transform applies the Mertz phase correction and the Norton−Beer apodization to the interferogram. Spectra were obtained in absorbance mode with an automatic background subtraction. Infrared spectra were acquired in the mid-IR region (wavenumbers from 450 to 5200 cm^{-1}) with a resolution of 2 cm^{-1} and using a KBr beamsplitter. Twenty-five scans of two seconds each were collected during the measurement of each sample, and the resulting absorbance spectrum for each sample was calculated from the average of the repeat scans. Figure 2 shows the IR spectra of a kerogen and bitumen isolate prepared using the methods described above. The kerogen sample was prepared with mass proportions of 1:900, 2:900, 5:900, and 10:900 mg [kerogen:KBr]; the bitumen sample was prepared with mass proportions of approximately 1:900, 3:900, and 5:900 mg [bitumen:KBr]. The intensity of the IR absorbance varies linearly with the mass/concentration of the sample, such that when the IR spectra are normalized by mass, the IR absorbance spectra practically overlay. These data confirm that both the kerogen and bitumen spectra obey the Beer−Lambert law and can be interpreted absolutely.

Absorbance Band Assignment. Following the acquisition of quantitative IR spectra, absorbance band characterization was carried out using a series of curve-fitting procedures. The spectral regions of particular interest for interpretation were the interval regions between 1500 and 1800 cm^{-1} and between 2800 and 3100 cm^{-1}. The part of

DOI: 10.1021/ef5027532
Energy Fuels 2015, 29, 2197−2210

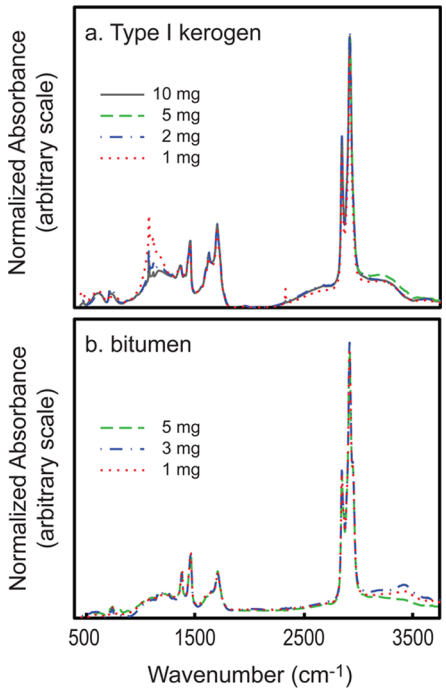

Figure 2. Infrared absorbance spectra normalized to mass of immature kerogen (a) and bitumen (b) prepared as KBr pellets with mass concentrations (mass of sample per 900 mg of KBr) as indicated in the plots. The measured absorbances scale linearly with mass/concentration and practially overlay across the range of wavenumbers of interest. Curve-fitting removes residual differences in the baseline spectrum such as the broadband absorbance between wavenumbers above 2500 cm^{-1} attributable to sorbed water.

the IR spectra between 700 and 900 cm^{-1} is commonly considered in the analysis of coals, but that part was not quantified here owing to the very low absorbance intensities observed in the IR spectra. Extensive investigations of coals, kerogens, and model organic compounds have enabled the assignment of IR absorbance bands to the vibrations of specific molecular functional groups.[10−13,15,34,35] Table 1 summarizes the band assignments.

The 1500 to 1800 cm^{-1} region contains overlapping absorbance bands associated with vibrations of aromatic ring and oxygenated functional groups.[10−13,15,35] Oxygenated functional groups include carboxyl (1575 cm^{-1}) and carbonyl (quinone, 1650 cm^{-1}; aldehyde/ketone, 1710 cm^{-1}; and ester, 1770 cm^{-1}). The broad absorbance 1600−1630 cm^{-1} can be resolved as two distinct peaks in the spectra of some organic materials centered at 1610 and 1630 cm^{-1}, both of which have been ascribed predominantly to aromatic ring stretching.

Absorbance bands in the IR spectra of organic materials between 2800 and 3000 cm^{-1} are associated with the stretching of aliphatic C−H bonds.[10−13,15] Five discrete peaks have been resolved[11,15] corresponding to CH (2897 cm^{-1}), CH_2 symmetric (2857 cm^{-1}), CH_2 asymmetric (2925 cm^{-1}), CH_3 symmetric (2872 cm^{-1}), and CH_3 asymmetric stretching (2962 cm^{-1}). Painter et al.[11] consider that the absorbance band at 2925 cm^{-1} in the IR spectra of coals is a composite of CH_2 and of CH_3 groups attached directly to an aromatic ring. Vibrations of aromatic C−H bonds appear as a broad absorbance band between wavenumbers 3000 and 3100 cm^{-1}.

Band Fitting of IR Spectra. Several contributions have reviewed procedures to obtain robust and scientifically meaningful fits to IR spectra.[11,36,37] The IR intervals of interest were first baseline-normalized to define the appropriate envelopes for the curve fitting. The baseline adjustment between 1500 and 1800 cm^{-1} was a straight line between the limits of that interval. The baseline adjustment between wavenumbers 2800 and 3100 cm^{-1} was a polynomial fit that allowed for a nonlinear baseline arising from the tail of broadband water and/or hydroxyl absorbance above 3300 cm^{-1}. The polynomial

Table 1. Band Assignment for IR Spectra of Organic Compounds

peak center[a] (wavenumber, cm^{-1})	assignment
700−900	C−H out-of-plane bending
720	aliphatic CH_2
750	aromatic, four neighboring C−H
820	aromatic, two neighboring C−H
870	aromatic, isolated C−H
1450−1460	aliphatic (±aromatic) CH_2 and CH_3 bending
1500−1800	carbon−carbon and carbon−oxygen stretching
1575	carboxyl COOH
1610	aromatic C═C (±shifted CO?)
1630	aromatic C═C (±phenol OH?)
1650	carbonyl (quinone) C═O
1710	carbonyl (ketone) C═O
1770	carboxyl (ester) C═O and C−O
2800−3100	C−H stretching
2857	aliphatic CH_2, symmetric
2872	aliphatic CH_3, symmetric
2897	aliphatic CH
2925	aliphatic CH_2, asymmetric
2962	aliphatic CH_3, asymmetric
3050	aromatic C−H

[a]Peak centers are assigned within a spectral window of ±10 wavenumbers.

used for baseline interpolation between 2800 and 3100 cm^{-1} was computed from a fit through the IR spectra extending to lower and higher wavenumbers (2400−2750 cm^{-1} and 3100−3260 cm^{-1}). A linear baseline adjustment would not alter in a meaningful way the results of the curve-fitting algorithm, but the fits are less robust.

For complex materials such as kerogen and bitumen, a Lorentz function, which describes the shape of spectral bands in homogeneously broadened materials, does not provide the best fit to IR spectral absorbance bands.[11,36] A Lorentzian distribution tends to overweight the extremes of the distribution (Figure 3). The change of the curve shape in the IR spectra of complex materials is ascribed to vibrational interactions between neighboring components of the material.[11] One method to fit absorbance bands in complex materials is by the use of a pseudo-Voigt function, which is a linear summed function of Lorentzian and Gaussian distributions [i.e., $f \times L + (1 - f) \times G$; $0 \leq f \leq 1$] where f is the parameter indicating the relative fraction of Lorentzian character for the fit and is a free parameter. The Lorentzian and Gaussian distributions take the common forms

$$L(x; x_0, \gamma, E) = E \cdot \frac{\gamma^2}{(x - x_0)^2 + \gamma^2}$$

and

$$G(x; x_0, \gamma, E) = E \exp\left\{-\left[\frac{(x - x_0)^2}{2(\gamma/1.1774)^2}\right]\right\}$$

The curve fitting procedure solved by a least-squares iterative procedure includes the peak center (mean value of the distribution, x_0), peak amplitude (E), peak half-width (scale parameter, γ), and f for all absorbance bands in each interval region. Generally, the peak centers are well-known and solutions were within 2 or 3 cm^{-1} of the initialization. Peak areas, I, were integrated from the peak fits. Meier[37] discussed the limitations of such an approach. In addition, Maddams[36] and Painter et al.[11] examined whether absorbance bands can show asymmetric character and concluded that skewed distributions should be used only when there are a priori reasons to do so; we did not consider asymmetric properties in the curve fitting of IR spectra.

FTIR Structural Parameters. Curve fitting of the absorbance bands in IR spectra between 1500−1800 cm^{-1} and 2800−3100 cm^{-1}

DOI: 10.1021/ef5027532
Energy Fuels 2015, 29, 2197−2210

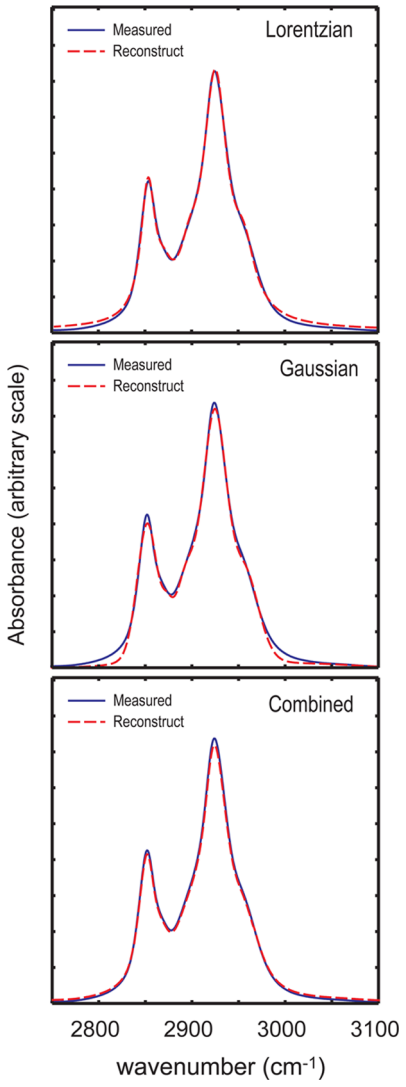

Figure 3. Lorentzian and Gaussian curve functions. The area under each of the curves is the same. Long tails characterize Lorentzian functions. (a) Lorentzian functions overfit the tails of measured absorbance bands of natural kerogen. (b) Gaussian functions underfit the same tails. (c) A combination of Lorentzian−Gaussian curve functions provides the better statistical reconstruction of the measured IR spectra of complex organic materials.

enabled the computation of several parameters describing the structural characteristics of both bitumen and kerogen.

CH_3/CH_2 Ratio. The methyl-to-methylene ratio[15,19] provides an indicator of aliphatic chain length and/or the degree of branching of aliphatic moieties. The CH_3 and CH_2 intensities used in the computation were the integrated peak areas arising from the prominent asymmetric stretching vibrations centered at 2957 and 2925 cm^{-1}, respectively, i.e., $CH_3/CH_2 = I_{2957}/I_{2925}$.

A-Factor. The A-factor expresses changes in the integrated intensities of IR absorbance bands from aliphatic C−H_x relative to aromatic C═C stretching vibrations[13,16,35] and so is one indicator of the relative aliphatic versus aromatic content of the sample. The A-factor is equal to $[I_{2857} + I_{2925}]/[I_{2857} + I_{2925} + I_{1600-1630}]$, where I_{2857} and I_{2925} are the integrated peak intensities of aliphatic CH_2 vibrations and $I_{1600-1630}$ is the integrated peak intensity of the aromatic C═C vibrations centered at 1610 and 1630 cm^{-1}.

C-Factor. The C-factor represents the intensity of the absorbance band related to vibrations of oxygenated functional groups versus aromatic ring functional groups[13] and so is an indicator of the relative oxygen content of the sample. Following convention, the C-factor was computed to be equal to $I_{1710}/[I_{1710} + I_{1600-1630}]$, where I_{1710} is the peak area resulting from the ketone C═O stretching vibration and $I_{1600-1630}$ is as defined above.

Aromaticity. We use the term aromaticity here as a qualitative proxy for the aromatic versus aliphatic carbon content of the samples. Aromaticity, as used here, is related to the relative peak intensity of aliphatic C−H_x versus aromatic C−H stretching modes between wavenumbers 2800 and 3100 cm^{-1} as defined by Painter et al.,[11] Fuller et al.,[38] Wang and Griffiths,[12] and Iglesias et al.[16] Aromaticity was calculated as $I_{3000-3100}/I_{2800-3000}$, where $I_{3000-3100}$ represents the integrated peak area of the broad aromatic C−H stretch and $I_{2800-3000}$ represents the sum area of the five aliphatic stretch vibrations. The definition of aromaticity here differs from that used commonly in nuclear magnetic resonance (NMR) spectroscopy, where aromaticity (or aromatic content) defines the relative fraction of carbon that is present in aromatic ring structures.

Degree of Condensation. According to Ibarra et al.,[17] the number of hydrogens directly bonded to ring structures indicates the degree of aromatic substitution versus ring condensation. Chen et al.[21] defined the degree of aromatic ring condensation, DOC1, as the ratio of peak intensity at 3000−3100 cm^{-1} divided by the peak intensity at 1600 cm^{-1}. This ratio reflects the relative intensity of IR absorbance bands arising from aromatic C−H stretching versus aromatic ring C═C stretching. Following this definition, DOC1 is computed as the ratio $I_{3000-3100}/I_{1600-1630}$ with these indices as defined above. The DOC1 decreases, according to this definition, as the extent of ring condensation increases. A caveat of interpreting DOC1 is that this parameter can vary without condensation of aromatic rings owing to changes in the intensity of the aromatic C−H stretch, for example, by replacement of aliphatic carbons bonded on aromatic rings with protons.

RESULTS

Composition of the Kerogen Concentrate. Isolation of kerogen required extensive treatment with concentrated acids to remove inorganic mineral components. The method used here for the isolation of kerogen followed that developed for Green River oil shale and which is demonstrated to have minimal impact on the structure and resulting IR spectral characteristics of the kerogen.[29] To examine if the acid treatment affected in a meaningful way the structure and composition of kerogen, we performed an identical acid treatment on solid asphaltene extracted from crude oil as a proxy for kerogen. The IR spectrum of the asphaltene sample was taken prior to and after the acid treatment using the identical methods for sample preparation and analysis used for the study of kerogens. Figure 4 compares the absolute IR spectra of the native and acid-treated asphaltene samples. The spectra practically overlay, indicating that the acid treatment does not affect the IR spectra and, by implication, the structural characteristics of the organic phase.

The purity of the kerogen concentrates was confirmed by the measurement of the isolates using X-ray fluorescence spectroscopy recognizing that this method has not been optimized for organic matrices. The concentrations of major mineral-forming elements Si, Al, Ca, Mg, K, Na, P, and Ti were below 0.2 wt %, confirming the effective removal of carbonate, clay, and siliciclastic minerals, as well as any neoformed fluorosilicates, during the acid treatment. The XRF data indicated residual pyrite in kerogen, which is common in kerogen concentrates isolated by the acid treatment used here,[29] by measurable and nearly equal weight concentrations of Fe and S (average 7.6 ± 1.7 wt % Fe, 9.6 ± 2.0 wt % S). Table 2 reports the atomic H/C ratio of the kerogens determined by elemental analysis. The H/C ratio of kerogen is unaffected by the presence of pyrite in the concentrate. Figure 5 plots the atomic H/C ratio of kerogen

DOI: 10.1021/ef5027532
Energy Fuels 2015, 29, 2197−2210

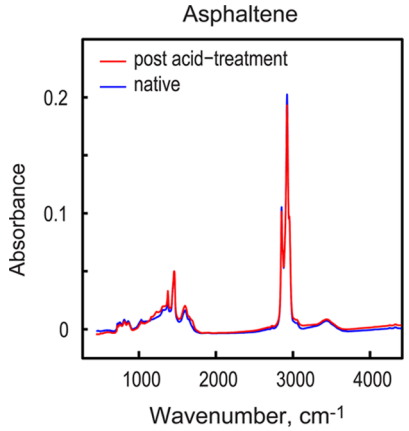

Figure 4. Comparison of the IR spectra of asphaltene prior to (native) and postacid treatment. The nearly identical spectra indicate that the acid demineralization procdure used for the isolation of kerogen from shale does not affect the IR spectral characteristics and, by implication, the structure and composition of the solid organic phase.

Table 2. Kerogen Maturity and Atomic H/C

sample EASY%Ro	atomic H/C
0.48	1.30
0.75	1.37
0.83	1.36
0.90	1.20
0.95	0.98
1.19	0.88
1.28	0.70

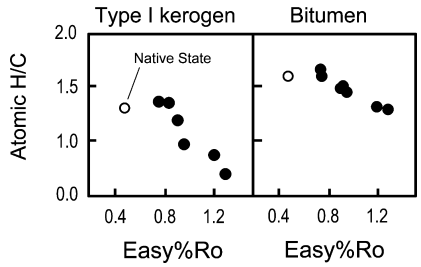

Figure 5. Atomic H/C ratios measured in type I kerogen and bitumen. The native state kerogen and bitumen are shown by the open symbols in this and subsequent figures.

versus thermal maturity. The atomic H/C ratio was 1.30 in the native state kerogen (EASY%Ro = 0.48%), 1.37 in the thermally immature samples (EASY%Ro = 0.75%), and significantly lower (0.70) in the most mature kerogen studied (EASY%Ro = 1.28%).

Composition of the Bitumen Extract. Unlike the kerogen isolate, the bitumen extract contains no inorganic impurities. The atomic H/C ratio of bitumen (Table 3) trends lower from 1.61 in the native state bitumen (EASY%Ro = 0.48%) to 1.29 in the most mature bitumen (EASY%Ro = 1.28%). Bitumen shows a trend with thermal maturity nearly parallel to that observed in the kerogens, but bitumen has systemically greater atomic H/C ratio (Figure 5).

Absolute FTIR Spectra. Figures 6 and 7 plot for the kerogen and bitumen series, respectively, their broadband IR spectra in order of increasing thermal maturity. The absorbance scale for the two sets of plots is absolute and the same. Several

Table 3. Bitumen Maturity and Atomic H/C

sample EASY%Ro	atomic H/C
0.48	1.61
0.74	1.71
0.75	1.60
0.90	1.49
0.92	1.51
0.95	1.45
1.19	1.32
1.28	1.29

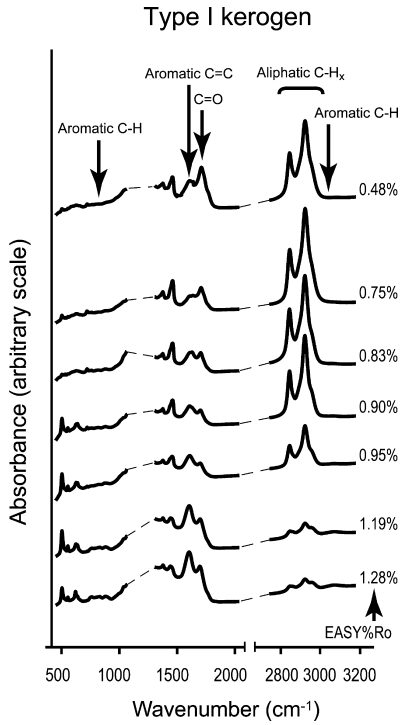

Figure 6. Quantitative IR spectra of kerogen plotted in order of thermal maturity. Band absorbances are indicated for vibrations of key organic functional groups. The following trends with thermal maturity are visible in the succession of IR spectra: Carboxyl/carbonyl decreases, aliphatic C−H_x decreases, and aromatic C═C and C−H increase. Spectra are offset for clarity.

trends are observable in both series, reflecting changes in the gross structure of kerogen and bitumen during pyrolysis. In kerogen, IR absorbance related to the presence of C−O/C═O functional groups and aliphatic C−H_x groups decreases with thermal maturation. The former band (1710 cm^{-1}) appears to increase in the two most mature kerogens. The IR absorbance related to aromatic C═C ring (1600−1630 cm^{-1}) and aromatic C−H vibrations (700−900 cm^{-1} and 3000−3100 cm^{-1}) increase during maturation.

The bitumen IR spectra show substantially greater absorbance peaks related to vibration of aliphatic C−H_x groups. The intensity of these peaks decreases with thermal maturity. The IR absorbance associated with C−O/C═O functional groups is small in most of the bitumen samples, except for in the bitumen sample with EASY%Ro = 0.75%. The IR absorbance related to aromatic C═C ring and aromatic C−H vibrations both increase in bitumen during maturation, as is observed in kerogen, but the absolute intensities are smaller.

DOI: 10.1021/ef5027532
Energy Fuels 2015, 29, 2197−2210

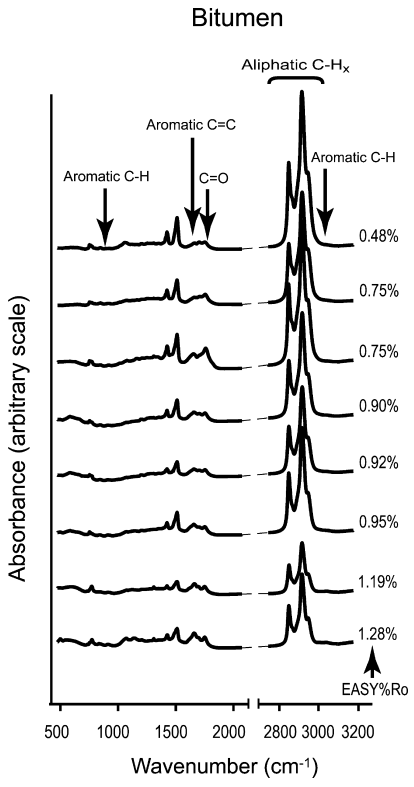

Figure 7. Quantitative IR spectra of bitumen plotted in order of thermal maturity. Band absorbances are indicated for vibrations of key organic functional groups. Bitumen relative to kerogen expresses higher aliphatic C−H_x, lower carboxyl/carbonyl, and lower aromatic C═C and C−H band abosrbances. Spectra are offset for clarity.

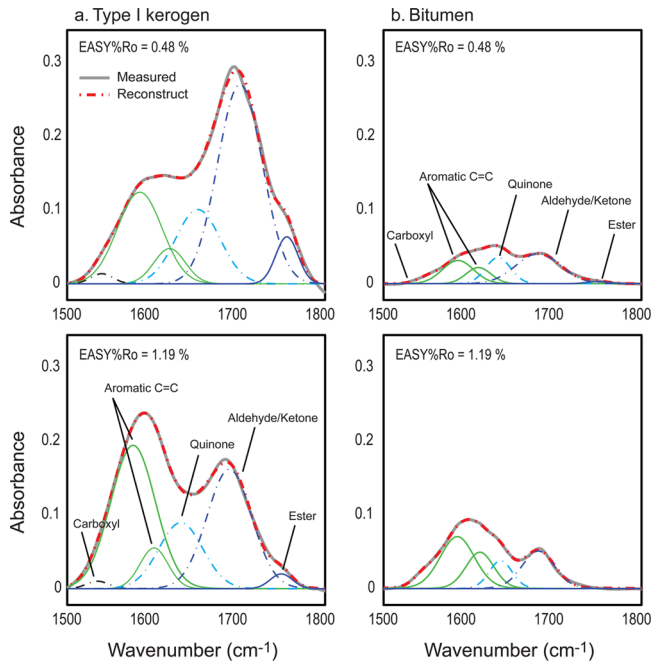

Figure 8. Six-curve fit and spectral reconstruction for IR spectra of type I kerogen (a) and bitumen (b) across wavenumber region 1500−1800 cm^{-1}. Illustrative spectra are shown for immature native state kerogen and bitumen (EASY%Ro = 0.48%) and an example of a thermally matured kerogen and bitumen (EASY%Ro = 1.19%).

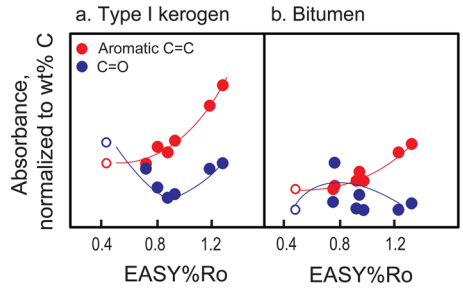

Figure 9. Integrated band intensities corresponding to aromatic C═C stretch (1610 cm^{-1}) and aldehyde/ketone C═O stretch (1710 cm^{-1}) plotted as a function of maturity for kerogen (a) and bitumen (b). Band absorbances are normalized to weight organic carbon (Table 2). Both bitumen and kerogen show an increase in IR absorbance related to aromatic C═C stretch with maturity. Trend lines are guides to the eye.

Curve fitting of the IR spectra in key absorbance regions (1500−1800 cm^{-1}; 2800−3100 cm^{-1}) enabled the changes in the IR spectra of kerogen and bitumen as a function of thermal maturity to be quantified and compared. Figure 8 compares the curve fits and spectral reconstructs of the IR spectra between 1500 and 1800 cm^{-1} (aromatic C═C and oxygen functional groups) for native state kerogen and bitumen and for one example of pyrolyzed kerogen and bitumen (EASY%Ro = 1.19%). Differences in the absolute IR absorbance of aromatic C═C and oxygen functional groups are clearly shown within the kerogen and bitumen fractions, as well as between the kerogen and bitumen series. Figure 9 quantifies for all kerogen and bitumen samples the integrated band absorbance of the aromatic C═C vibration and C═O vibration (ketone/aldehyde). The fits demonstrate for both series the relative increase with increasing maturity in the abundance of aromatic ring functional groups relative to oxygen functional groups. The absolute intensity of aromatic C═C absorbance in bitumen is lower than that in kerogen. The data also reveal subtle trends including an increase in the abundance of oxygen functional groups in the most mature kerogens (EASY%Ro ≥ 1.2%) and a peak in the abundance of oxygen functional groups in low-maturity bitumen (EASY%Ro = 0.75%).

Figure 10 shows curve fits for the wavenumber region 2800−3100 cm^{-1} (aliphatic C−H_x and aromatic C−H absorbance bands); the fits are shown for the same native state and pyrolyzed kerogen and bitumen presented in Figure 8. The fits show that IR absorbance owing to aliphatic C−H_x vibrations is greater in the native state than in the thermally mature fraction. The IR absorbance band related to aromatic C−H vibrations is resolvable in the pyrolyzed samples but not in the native state. The absolute intensity of the IR peaks associated with aliphatic C−H_x vibrations are greater in bitumen than in kerogen. Figure 11 quantifies for the kerogen and bitumen series the integrated absorbance for the sum of five aliphatic C−H_x bands and the broad aromatic C−H band. The data confirm the higher aliphatic C−H absorbance of the bitumen versus the kerogen. The aliphatic C−H_x absorbance declines in both bitumen and kerogen during pyrolysis. In detail, the pyrolyzed kerogens express a peak at low maturity (EASY%Ro ∼ 0.75%) in the IR absorbance of aliphatic C−H_x functional groups. This trend has been documented previously in kerogen macerals of varying thermal maturity.[15] The IR absorbance related to the presence of aromatic C−H is not resolvable at low thermal maturity (EASY%Ro < 0.9%) in either the kerogen or bitumen. The

DOI: 10.1021/ef5027532
Energy Fuels 2015, 29, 2197−2210

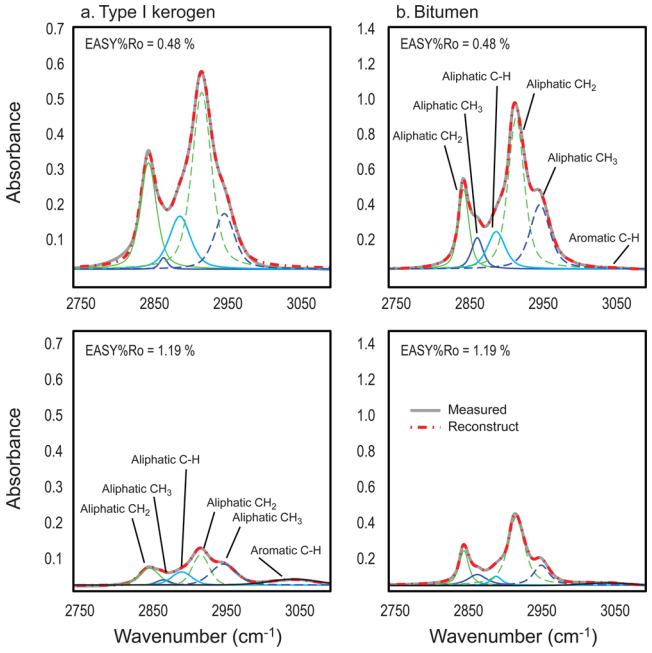

Figure 10. Six-curve fit and spectral reconstruction for IR spectra of type I kerogen (a) and bitumen (b) across wavenumber region 2700–3100 cm^{-1}. Illustrative spectra are shown for immature native state kerogen and bitumen (EASY%Ro = 0.48%) and an example of a thermally matured kerogen and bitumen (EASY%Ro = 1.19%).

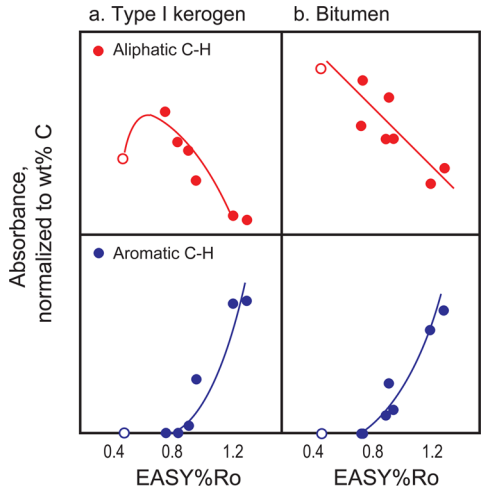

Figure 11. Integrated band intensities corresponding to aliphatic C–H_x stretch (2800–3000 cm^{-1}) and aromatic C–H stretch (3000–3100 cm^{-1}) plotted as a function of maturity for kerogen (a) and bitumen (b). Band absorbances are normalized to weight organic carbon (Table 2). Trend lines are guides to the eye. The scatter in the trend for bitumen of aliphatic C–H_x versus EASY%Ro may partially reflect an artifact of the normalization, assuming exactly 1.000 mg of bitumen in solution was transferred to the KBr mixture.

appearance of this band coincides with the significant decline of the aliphatic C–H_x bands in both organic fractions.

FTIR Structural Parameters. Figure 12 compares for the series of pyrolyzed kerogen and bitumen samples the FTIR structural indices quantified in this paper as a function of their thermal maturity. Panels a and b of Figure 12 plot the CH_3/CH_2 ratio for kerogen and bitumen, respectively. Pyrolysis of kerogen resulted in only a small decrease in the CH_3/CH_2 ratio at low thermal maturity (EASY%Ro ~ 0.9%), and the trend is

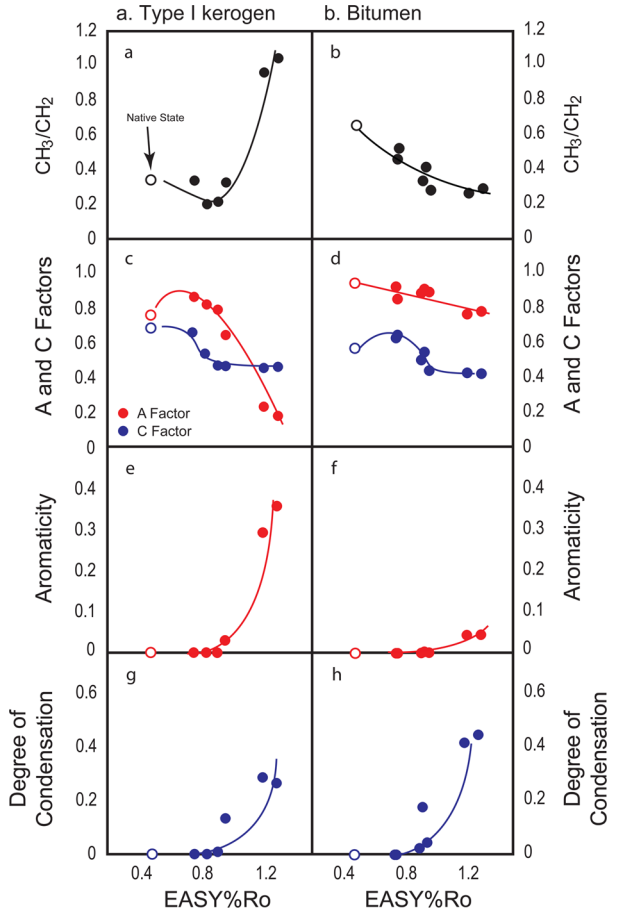

Figure 12. FTIR structural parameters for the interpretation of alteration trends in kerogen and bitumen during pyrolysis. Trends for kerogen are shown in the left panels; trends for bitumen are shown in the right panels: aliphatic CH_3/CH_2 ratio plotted in (a) and (b); A-factor (aliphatic C–H_x/aromatic C=C) and C-factor (ketone/aldehyde C=O/aromatic C=C) plotted in (c) and (d); aromaticity index (aromatic C–H/aliphatic C–H_x) plotted in (e) and (f); degree of condensation (aromatic C–H/aromatic C=C) plotted in (g) and (h). The parameters confirm both differences (evolution of CH_3/CH_2 ratio, A-factor, and C-factor, absolute aromatic content) and similarities (degree of condensation, increasing aromaticity during maturation) in the alteration of bitumen and kerogen. Lines are guides to the eye.

not systematic. The CH_3/CH_2 ratio of kerogen increased significantly at higher thermal maturity (EASY%Ro ≥ 1.2%). Bitumen expresses behavior different from that of kerogen. The CH_3/CH_2 ratio is highest in the native state bitumen and decreases nearly monotonically during thermal maturation. The same CH_3/CH_2 trend in bitumen was also documented using ^{13}C NMR spectroscopy for the same series of samples,[25] at least within the range of thermal maturity examined here.

Panels c and d of Figure 12 plot the A- and C-factors for the series of kerogens and bitumens, respectively. The A-factor relates the relative abundance of aliphatic C–H_x to aromatic C=C functional groups. Pyrolysis results in a maximum in the A-factor of kerogen at low maturity (EASY%Ro ≤ 0.9%), followed by a significant decrease at higher thermal maturity. Studies of the IR spectra of coals document similar trends with coal rank.[16,21] The A-factor for bitumen is systematically greater than that for kerogen and decreased monotonically with increasing thermal maturity. The C-factor is a proxy for the

DOI: 10.1021/ef5027532
Energy Fuels 2015, 29, 2197–2210

relative abundance of oxygenated versus aromatic C=C functional groups. The C-factor for kerogen decreased during pyrolysis, with the decline occurring acutely at low thermal maturity, EASY%Ro < 0.8%. This trend follows those documented for coal[21] and other kerogens.[19] The C-factors for bitumen trend similar to that expressed by the pyrolyzed kerogen; however, the C-factor has a maximum in the bitumen sample with EASY%Ro = 0.75%.

Panels e and f of Figure 12 plot the aromaticity index, the ratio of peak intensities related to aliphatic C−H_x versus aromatic C−H vibrations, for the series of kerogens and bitumens, respectively. Aromaticity is low in both the kerogen and bitumen samples with maturity EASY%Ro < 1%. Here, unquantifiable absorbance associated with aromatic C−H vibrations in low-maturity samples does not indicate the absence of aromatic structures (i.e., aromatic C=C bonds). Bitumen shows the same trend of increasing aromaticity index with thermal maturity. Absolute aromaticity is significantly lower in bitumen than in kerogen for any EASY%Ro value.

Panels g and h of Figure 12 plot the degree of condensation, DOC1, in kerogen and bitumen, respectively. The DOC1 reflects the ratio of the intensity of IR absorbance bands arising from aromatic C−H stretching to aromatic C=C ring stretching. DOC1 increases with thermal maturity in both kerogen and bitumen, with the evolution similar in both organic fractions. The trends follow that observed in low-rank coals, VRo < 2%.[21] Condensation trends in coals with VRo > 2%, much beyond the range of thermal maturities examined here, show a subsequent decrease in DOC1.

DISCUSSION

The products of thermal maturation of kerogen comprise bitumen, petroleum (i.e., oil and associated hydrocarbon gases), and nonhydrocarbon gases. Bitumen can act as a reaction intermediary in the generation of petroleum, being preferentially formed at low thermal maturity and subsequently consumed at higher thermal maturity by cracking.[8,39] In this framework, bitumen may share similar structural characteristics with kerogen because bitumen represents lower molecular weight units cleaved from macromolecular kerogen. In support, Salmon et al.[40] using NMR spectrometry reported similarity between kerogen and bitumen with respect to carbon backbone structures. On the other hand, Pomerantz et al.[41] have shown using X-ray absorption near edge structure (XANES) analysis that kerogen and bitumen can differ at least in terms of the bonding environments of sulfur, with kerogen enriched in reduced and nonpolar forms of sulfur and bitumen dominated by polar sulfoxide. This result suggests differences between kerogen and bitumen in the distribution of at least some molecular moieties.

Whereas there are numerous IR spectroscopy studies on the structural characteristics of kerogen, relatively few studies have investigated bitumen structure during thermal maturation, despite the importance of bitumen in the generation of oil and gas. Here, we used a novel sample preparation to acquire quantitative IR spectra of bitumen, which enabled changes in the structure of bitumen to be studied and compared directly to that of kerogen under the same maturation conditions. To our knowledge, no such comparison exists. The IR results show that the structure and composition of bitumen is not uniform during maturation. Moreover, the IR data reveal differences in the distribution and abundance of specific molecular functional groups between bitumen and kerogen during the maturation process, indicating that structural alteration of these organic components is not all the same. We separately discuss structural changes in kerogen and bitumen occurring in the maturity range where bitumen is predominantly being formed (EASY% Ro < 0.9%) and subsequently consumed (EASY%Ro > 0.9%).

Alteration of Kerogen at Artificial Maturity Level EASY%Ro < 0.9%. Thermal alteration of kerogen at low maturity is driven predominantly by the loss of oxygen functionality (e.g., decarboxylation) as inferred by the sharp decline in IR absorbance associated with C−O and C=O functional groups. Early loss of oxygen functional groups is revealed by the acute decrease in the C-factor for low-maturity samples with an EASY%Ro less than 0.9% (Figure 12c). There is no clear evidence to support that one or the other functional groups is preferentially lost. The loss of oxygen functional groups at low maturity rank is consistent with the results of Tissot et al.[22] describing in the Green River formation a decrease in carboxyl and carbonyl content of kerogen at shallow stratigraphic depths and has been documented in a range of other kerogens and organic macerals during natural and artificial maturation.[13,15,19,35,42] Furthermore, Burnham et al.[43] in their laboratory study of biomarkers from the Green River inferred that early isoprenoid pyrolysates had compositions consistent with decomposition of oxygen-containing acids and esters in kerogen. The IR data suggest that the oxygen is partially incorporated into bitumen (at least at the lowest maturity; discussed below), but a significant fraction must also be lost to the gas component (e.g., CO_2, CO) during pyrolysis. Previous studies have also shown that the generation of nonhydrocarbon gases occurs prior to the onset of major oil and hydrocarbon gas generation, supporting the notion of early decomposition of oxygen functions in kerogen.[22,44]

Within the same maturity range, IR absorbance related to vibrations of aliphatic carbon changes less dramatically and after changes associated with oxygen functional groups. For example, the A-factor (Figure 12c) decreases only modestly up to artificial maturity level EASY%Ro < 0.9%. The A-factor (aliphatic versus aromatic) and C-factor (oxygenated versus aromatic functional groups) can be compared in a pseudo van Krevelen diagram[13] analogous to the well-known plot of kerogen H/C versus O/C. Figure 13 plots these parameters for the kerogen samples, with the data points distinguished by thermal maturity. The plot demonstrates the clear decrease in the C-factor concurrent with a smaller decrease in the A-factor, which nearly parallel changes observed in the van Krevelen H/C versus O/C composition space for type I kerogen. It is noteworthy that early decomposition of carboxyl and carbonyl functions is generally consistent with known bond dissociation energies.[45,46] For example, the bond dissociation energy for the C−O bond in the ester moiety of $CH_3C(O)-OC_6H_5$ is only ~320 kJ/mol, whereas the bond dissociation energy for the C−C bond between the α carbon and the aromatic ring for $CH_3-C_6H_5$ is ~430 kJ/mol.[46] Early structural changes in kerogen during maturation can be illustrated by chemical reactions such as

$$R-C(O)O-R \rightarrow R-R + CO_2 \quad (2)$$

$$R-CO-R \rightarrow R-R + CO \quad (3)$$

$$R-C(O)O-R' + H_2 \rightarrow R-H + R'-H + CO_2 \quad (4)$$

$$R-CO-R' + H_2 \rightarrow R-H + R'-H + CO \quad (5)$$

DOI: 10.1021/ef5027532
Energy Fuels 2015, 29, 2197−2210

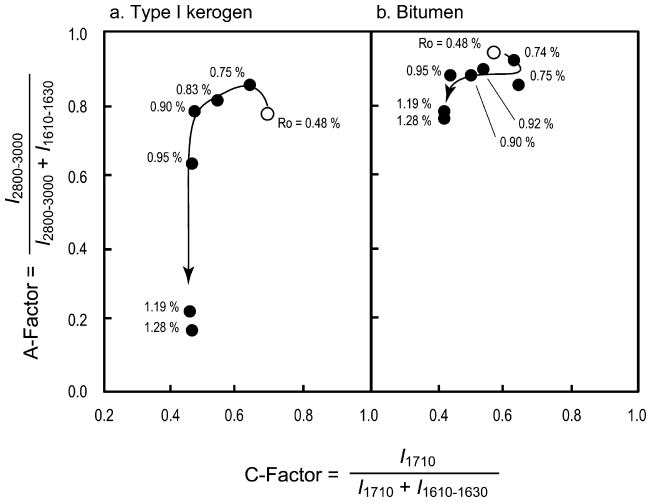

Figure 13. Pseudo van Krevelen diagram illustrating the evolution of aliphatic (A-factor) and oxygen functional groups (C-factor) in kerogen (a) and bitumen (b) as a function of thermal maturity (EASY%Ro from 0.48 to 1.28%). The A- and C-factors are IR proxies for atomic H/C and O/C ratios plotted on a standard van Krevelen diagram. The IR data demonstrate that early thermal alteration of kerogen is driven by loss of oxygenated functional groups, whereas later thermal alteration is dominated by loss of aliphatic carbon. Bitumen shows differences in its structural alteration including an early peak in oxygenated functional groups owing to oxidation, systematically higher aliphatic content, and overall smaller extents of structural alteration.

In these reactions, R represents the kerogen macrostructure with a framework of aromatic structures and R′ is a fragment that yields the pyrolysate (i.e., bitumen, oil, and hydrocarbon gas). In the instance that a fraction of the organic oxygen in kerogen is incorporated into bitumen, a relevant reaction can be illustrated as

$$\mathrm{R{-}CO{-}R' + H_2 \rightarrow R{-}H + R'{-}COH} \quad (6)$$

In all cases, the residual kerogen at low thermal maturity is depleted in O/C relative to the precursor.

The trends in the IR spectra and in IR structural parameters give no evidence of substantial changes in the structure or distribution of the aromatic carbon skeleton in kerogen at low maturity. For example, the absolute intensity of the aromatic C═C absorbance band (Figure 9), the aromatic C−H absorbance band (Figure 11), and the aromaticity index (Figure 12e), are all essentially unchanged for EASY%Ro < 0.9%.

Alteration of Kerogen at Artificial Maturity Level EASY%Ro > 0.9%. The predominant trends in the IR absorbance spectra of pyrolyzed kerogen for samples with artificial maturity above EASY%Ro > 0.9% reflect a dramatic decrease in aliphatic carbon and increase in aromatic carbon functional group abundance. These changes are consistent with trends observed among major kerogen types buried in sedimentary strata in which the decrease in the IR absorbance of aliphatic C−H_x groups and appearance of aromatic C−H bands in kerogen occurs coincidentally and in deeply buried stratigraphic units below those in which oxygen functional groups are decomposed.[22,34,35] Our results also parallel those findings of the alteration of kerogen during laboratory maturation.[34,42] The loss of aliphatic functional groups is reflected geochemically in our kerogen samples by the decrease in the atomic H/C ratio (Figure 5). The loss of aliphatic C−H_x structures coincides with the onset of major oil (±hydrocarbon gas) generation as indicated by the distribution and abundance of pyrolysates in these experiments (Figure 1). This process is driven by the cleavage of carbon−carbon bonds in aliphatic chains from the kerogen macrostructure. The produced aliphatic and hydrogen-rich molecules are the pyrolysates, the complement to which is the relatively hydrogen-poor kerogen residue characterized by an acute decline in aliphatic C−H_x content.

Bond dissociation energies favor cleavage of the aliphatic carbon−carbon bonds between the α and β position.[45,46] This mechanism leaves a residual methyl group attached to the aromatic ring structure in kerogen. The bulk CH_3/CH_2 ratio of kerogen also increased sharply in this maturity range (Figure 12a). Changes in the methyl-to-methylene ratio[15,19] reflect a change in the average aliphatic chain length and/or in the degree of chain branching (branched versus normal structures). Here, we interpret the loss of aliphatic C−H_x and increase in CH_3/CH_2 ratio to reflect shortening of aliphatic chain lengths in response to the carbon−carbon bond cleavage described above.

There is in the most thermally mature kerogen a marked increase in the IR absorbance associated with aromatic C═C ring structures (1610−1630 cm^{-1}; Figure 9) and the first appearance of the IR absorbance bands related to aromatic C−H vibrations (Figures 6 and 11). These changes are consistent with earlier results from IR spectroscopic studies on the maturation of kerogen.[10−12,19,22] The trends are also supported by independent solid-state ^{13}C NMR spectroscopy results that reveal an increase in the abundance of aromatic moieties in thermally mature versus immature kerogens from type I oil shale and other source rocks.[47−50] For example, Cao et al.[48] have interpreted the ^{13}C NMR spectra of Green River native and pyrolyzed kerogen as demonstrating an absence of protonated aromatic moieties in native kerogen combined with a detectable and significant fraction of protonated aromatic carbon in the postpyrolysis kerogen residue. These changes at relatively high thermal maturity in our pyrolysis experiments are coincident with major hydrocarbon gas (predominantly methane) generation. We interpret these changes as reflecting loss of methyl carbon structures (i.e., as methane) directly bonded to aromatic rings. At least some of this methyl carbon loss is via protonation of aromatic rings, as indicated by the appearance of IR absorbance bands from aromatic C−H vibrations at high thermal maturity. Bond dissociation energies for cleavage of a carbon−carbon bond between the α carbon and aromatic ring are significantly greater than for a carbon−carbon bond between the α and β carbons of an aliphatic chain;[45,46] hence, our interpretation is that methyl carbon loss dominates after the loss of longer aliphatic moieties.

Increase in aromatic content can also result from condensation (fusing) of aliphatic carbon into aromatic rings of increasing cluster size, as demonstrated to varying extents by solid-state ^{13}C NMR spectroscopic studies.[48−50] For IR spectroscopy, the degree of condensation (DOC1) has been used as a proxy for the extent of aromatic cluster growth during maturation of coals.[17,21] The DOC1 as defined (absorbance ratio of aromatic C−H to aromatic C═C) decreases during the process of condensation. In our study, DOC1 in kerogen increases during thermal maturation (Figure 12g). This trend gives no indication of condensation of aromatic rings. Instead, the trend implies that protonation of existing aromatic rings

DOI: 10.1021/ef5027532
Energy Fuels 2015, 29, 2197−2210

dominates over the potential condensation of new aromatic rings previously inferred from ^{13}C NMR studies. One consequence of increasing aromatic content in kerogen, irrespective of the mechanism, is the formation of residual kerogens at high thermal maturity with low atomic H/C ratio (~0.7; Figure 5).

An unexpected characteristic of the most mature kerogen samples is their apparent increase in oxygen content (Figure 9). Possibly, the oxidation of kerogen here is a unique consequence of maturation by laboratory pyrolysis because increasing oxygen content is generally not observed in naturally matured kerogen.[19] The mechanism for this enrichment is uncertain. One mechanism could be enrichment of oxygen during formation of pyrobitumen from alteration of bitumen. Bitumen maturation generates not only petroleum (oil and hydrocarbon gas) but also an inert residuum (pyrobitumen). In the pyrolysis experiments, pyrolyzable kerogen and all inert residues are operationally indistinguishable and measured as one in the kerogen isolate. This mechanism necessitates that the bitumen precursor to pyrobitumen be relatively rich in oxygen.

Alteration of Bitumen in Comparison to Kerogen. Bitumen in the pyrolysis experiments was formed from the thermal degradation of kerogen (Figure 1).[8] The IR spectra show that bitumen has a lower aromatic carbon (Figure 9) and higher aliphatic carbon content (Figure 11) than kerogen. The higher aliphatic content of bitumen inferred from IR data is consistent with the higher atomic H/C ratio of bitumen (Figure 5). In the pyrolysis experiments at low maturity where bitumen was predominantly being formed (EASY%Ro < 0.9%), the structural evolution of bitumen follows a maximum in oxygen content, as demonstrated by the peak in the absolute IR absorbance associated with oxygen functional groups (Figures 9 and 12d). The data imply that the earliest bitumen products contain oxygen, likely from organic oxygen in the primary kerogen (e.g., eq 6). These results are supported by the findings from the XANES study of the same bitumen samples, which revealed the highest concentration of highly oxidized sulfur moieties (sulfone, i.e., sulfur bonded to two oxygen atoms) in low-maturity bitumen that were not present in either the native state or thermally matured bitumen.[8] Pomerantz et al.[41] have independently documented by XANES on naturally matured organic-rich mudstones and shales the presence of other oxidized organic moieties in bitumen in the form of sulfoxide (sulfur double-bonded to a single oxygen) that are not present in native kerogen. The potential importance of this oxidation is the formation of a significantly more polar bitumen component in the rock, which alters the sorptive and/or solubility properties of the bitumen and may enhance expulsion of petroleum (oil and hydrocarbon gases) owing to their nonpolar character.[41]

The peak in the IR absorbance of C═O and C−O begins to disappear by artificial maturity levels EASY%Ro ~ 0.8%, implying decomposition of oxygen functional groups as bitumen starts to be converted during pyrolysis to oil, gas, and pyrobitumen. In this way, early maturation of bitumen bears one similarity to that of kerogen because both are driven by changes in the abundance of oxygen functional groups. Bitumen is still being formed from the maturation of kerogen at this stage (Figure 1); a second possibility for the lower oxygen content of bitumen present later in the pyrolysis experiments is that the kerogen itself from which bitumen is formed has lower oxygen content (Figure 9).

Bitumen is preferentially consumed at higher thermal maturity (EASY%Ro > 0.9%) as the generation of oil and hydrocarbon gas reaches a maximum (Figure 1). Trends in the IR spectra of bitumen at artificial maturity levels EASY%Ro > 0.9% indicate a decrease in aliphatic carbon content, an increase in the aromaticity index, and an increase in the degree of condensation (Figure 12). These trends follow those documented for kerogen previously and in this study (i.e., loss of aliphatic carbon and concentration of aromatic carbon), but the direct comparison of the IR spectra shows the magnitude of the changes differ. Data from Feng et al.[25] in a ^{13}C NMR study of the same series of bitumen samples support our interpretations; the NMR data show that the percentage of carbon in aromatic structures in bitumen increased systematically with thermal maturity from 13 to 48% (EASY%Ro = 0.48 to 1.28%). The aliphatic carbon content of bitumen is higher than that in the kerogen, as indicated by the A-factors. While the A-factor decreases in both fractions during maturation, the change in bitumen is small relative to that in kerogen, implying that the aromatic content of bitumen increases but remains lower in bitumen relative to that in kerogen at equivalent thermal maturity. The pseudo van Krevelen plot (Figure 13) clearly indicates the smaller change in the aliphatic versus aromatic content in bitumen versus in kerogen.

The aromaticity index suggests protonation of aromatic rings occurs with increasing artificial maturation levels as aliphatic chains are cleaved to yield oil and gas, a mechanism similar to that inferred for kerogen. However, absolute aromatic content is significantly lower in bitumen because the fraction of aromatic carbons (aromatic C═C; aromatic C−H) versus aliphatic carbons (aliphatic $C-H_x$) is low in bitumen relative to that in kerogen. It is notable that the DOC1 is similar for bitumen and kerogen; as such, we infer that the fraction of carbon in aromatic rings bound to hydrogen is nearly the same between the two fractions. Subtle increase in the degree of protonation of aromatic rings in bitumen can also be interpreted by the ^{13}C NMR study of these bitumen samples, although Feng et al.[25] limited the significance of their findings.

A key difference between the structures of bitumen and kerogen during the maturation experiments is their aliphatic CH_3 versus CH_2 contents during evolution. Bitumen exhibits a systematic decrease in the CH_3/CH_2 ratio throughout the range of thermal maturity considered in this study (Figure 12b). This trend is opposite to the well-known evolution in kerogen of increasing CH_3/CH_2 ratio,[15,19] also observed here. The monotonic decrease in CH_3/CH_2 with increasing thermal maturity during bitumen formation as shown by IR spectroscopy is the same as that shown by ^{13}C NMR spectroscopy,[25] at least up to the limit of thermal maturity (EASY%Ro ~ 1.3%) considered here. The increase in the abundance of methylene-versus-methyl groups indicates the lengthening on average and/or reduction in branching on average of aliphatic chains in bitumen during maturation. The ^{13}C NMR spectroscopy measurements on these samples[25] reveal a distribution of tertiary versus primary (methyl) and secondary (methylene) carbons in aliphatic chains, which were interpreted as reflecting both increasing chain length and decreasing degree of branching. Gas chromatography measurements of bitumen samples from these pyrolysis experiments indicate that bitumen becomes less branched with thermal maturity (A. Burnham, personal communication). Similarly, earlier studies of pyrolysates from laboratory pyrolysis have shown a reduction during maturation in the abundance of branched aliphatic compounds

DOI: 10.1021/ef5027532
Energy Fuels 2015, 29, 2197−2210

(e.g., isoprenoids) versus normal *n*-alkenes and *n*-alkanes.[43,51] In this regard, the evolution of aliphatic chains in kerogen and bitumen differs significantly in the range of maturity studied here: aliphatic chains in kerogen shorten during maturation, whereas those in bitumen become less branched and longer. At higher thermal maturity, beyond the range available for our study, Feng et al.[25] observed that the CH_3/CH_2 ratio trend with maturity reverses. The inference is that the average aliphatic chain length in bitumen becomes shorter during bitumen decomposition and intensive petroleum generation at high thermal maturity.

There exists little data concerning the IR spectral characteristics of bitumen against which we can compare directly our observed structural changes in bitumen during thermal maturation. However, several studies have reported the IR spectra of asphaltenes,[14,31,32] which are an important fraction of bitumen and as such may share similar structures and trends during maturation. The compositional trends reported in asphaltene as a function of thermal maturity are dominated by the relative decreasing abundance of oxygen functional groups and aliphatic carbon structures compared to aromatic carbon structures.[14,31,32] The first changes were interpreted as decarboxylation of the asphaltene structure. Thereafter, aromatization of the residual asphaltene structure dominated as aliphatic carbon structures are removed. In this regard, the structural trends in asphaltene isolates are broadly similar to those documented herein for bitumen. One of these studies[14] also compared the IR spectra of directly related kerogen and asphaltene samples. This comparison showed that asphaltenes relative to kerogens had greater aliphatic carbon and carboxyl/carbonyl (i.e., greater A- and C-factors) versus aromatic carbon contents. These relative differences between asphaltene and kerogen are very similar to those documented in this study between bitumen and kerogen (Figure 13).

■ CONCLUSIONS

A series of bitumen and kerogen samples of varying thermal maturity (EASY%Ro = 0.48−1.28%) were obtained by anhydrous, semi-open pyrolysis of Green River oil shale, and their structural properties were examined by Fourier transform IR spectroscopy. A new method was developed using cryomill sample preparation, which enabled quantitative IR spectroscopy of bitumen and absolute comparison with the IR characteristics of kerogen. We draw the following conclusions.

The IR spectra confirm the higher aliphatic and lower aromatic carbon content of bitumen versus kerogen at every artificial maturity level (A-factor, aromaticity index) as supported by other geochemical data (atomic H/C ratio).

At relatively low artificial thermal maturity (EASY%Ro ∼ 0.5 to 0.9%), prior to onset of major oil and hydrocarbon gas generation, alteration of both bitumen and kerogen is dominated by changes in oxygen abundance. Kerogen shows extensive loss of oxygen functional groups (decarboxylation) during early decomposition. In contrast, bitumen expresses a peak in the IR absorbance of oxygen functional groups before decarboxylation at higher maturity, which is supported by a peak in the oxygen content shown by independent X-ray spectroscopy studies of these samples.[8] Enrichment likely reflects incorporation of organic oxygen lost from kerogen. The IR spectra of kerogen (A-factor, aliphatic CH_3/CH_2 ratio) exhibit subtle enrichment at low maturity in aliphatic content and average length of aliphatic chains, an observation that is consistent with traditional geochemical data (e.g., peak in atomic H/C ratio). Bitumen does not show the same maximum in the A-factor.

Aliphatic chains in bitumen lengthen and/or become less branched during pyrolysis in the maturity range where bitumen is primarily being formed. This is in marked contrast to the well-known behavior of kerogen, which in the same range of thermal maturity shows decreasing alkyl chain length as kerogen is cracked to yield lower-molecular-weight pyrolysates including bitumen, oil, and gas.

At higher thermal maturity, during the principal phase of petroleum generation, kerogen and bitumen express increasing aromatic character. For kerogen, this appears to reflect loss of aliphatic-enriched fractions to the pyrolysates and concentration of aromatic carbon in the kerogen residue. Bitumen is both formed (from breakdown of kerogen) as well as decomposed (by oil and hydrocarbon gas generation and pyrobitumen formation at higher maturity) in the pyrolysis experiments. Increasing aromaticity in bitumen likely reflects both loss of aliphatic-enriched components in petroleum as well as inheritance of increasingly aromatic compositions from kerogen. These major structural changes in bitumen and kerogen can be clearly contrasted on pseudo van Krevelen diagrams plotting A-factors (aliphatic versus aromatic content) against C-factors (carboxyl/carbonyl versus aromatic content) as proxies for atomic H/C and O/C ratios.

Loss of aliphatic carbon (and probably other functional moieties) from aromatic centers is accommodated in both kerogen and bitumen by protonation of aromatic rings. The degree of protonation on aromatic rings in bitumen and kerogen appears to be very similar. The IR data provide no direct indication for condensation of aromatic rings in either kerogen or bitumen with increasing artificial maturation levels, but the mechanism is not excluded.

The most mature kerogen samples appear to show a late enrichment of oxygen. This may be a characteristic unique to thermal maturation via high-temperature pyrolysis. The mechanism for this enrichment is uncertain but could reflect concentration of oxygen in pyrobitumen from alteration of precursor bitumen with elevated oxygen content (pyrobitumen is operationally indistinguishable from kerogen in our experiments).

■ AUTHOR INFORMATION

Corresponding Author

*E-mail: pcraddock@slb.com.

Notes

The authors declare no competing financial interest.

■ ACKNOWLEDGMENTS

We acknowledge TOTAL, American Shale Oil (AMSO), and Schlumberger for support and permission to publish the results of this study. Alan Burnham (AMSO) and Stephen Larter (Schlumberger) are thanked for insightful comments and discussions on a draft of this manuscript. We thank the three anonymous reviewers for their constructive reviews of this work.

■ REFERENCES

(1) Burnham, A. K.; Singleton, M. F., High-pressure pyrolysis of Green River oil shale. In *Geochemistry and Chemistry of Oil Shales*; Miknis, F. P., McKay, J. F., Eds.; ACS Symposium Series 230; American Chemical Society: Washington, DC, 1983.

DOI: 10.1021/ef5027532
Energy Fuels 2015, 29, 2197−2210

(2) Cummins, J. J.; Robinson, W. E. *Thermal degradation of Green River kerogen at 150° to 350 °C*; U.S. Bureau of Mines Report of Investigations RI 7620; U.S. Bureau of Mines: Washington, DC, 1972.
(3) Bartis, J. T.; LaTourette, T.; Dixon, L.; Peterson, D. J.; Cecchine, G. *Oil shale development in the United States: Prospects and policy issues*. RAND Corp.: Santa Monica, CA, 2005.
(4) Shen, C. *Reservoir simulation study of an in-situ conversion pilot of Green River oil shale*. Presented at the Rocky Mountain Petroleum Technology Conference, Denver, Colorado, April 14−16, 2009; Paper SPE 123142; http://dx.doi.org/10.2118/123142-MS.
(5) Burnham, A. K.; Day, R. L.; Hardy, M. P.; Wallman, P. H. AMSO's novel approach to in-stiu oil shale recovery. In *Oil Shale: A Solution to the Liquid Fuel Dilemma*; Ogunsola, O. I., Hartstein, A. M., Ogunsola, O., Eds.; ACS Symposium Series 1032; American Chemical Society: Washington, DC, 2010.
(6) Ryan, R. C.; Fowler, T. D.; Beer, G. L.; Nair, V. Shell's in situ conversion process−From laboratory to field pilots. In *Oil Shale: A Solution to the Liquid Fuel Dilemma*; Ogunsola, O. I.; Hartstein, A. M.; Ogunsola, O., Eds.; ACS Symposium Series 1032; American Chemical Society: Washington, DC, 2010.
(7) Symington, W. A.; Kaminsky, R. D.; Meurer, W. P.; Otten, G. A.; Thomas, M. M.; Yeakel, J. D. ExxonMobil's ElectroFrac process for in situ oil shale conversion. In *Oil Shale: A Solution to the Liquid Fuel Dilemma*; Ogunsola, O. I., Hartstein, A. M., Ogunsola, O., Eds.; ACS Symposium Series 1032; American Chemical Society: Washington, DC, 2010.
(8) Le Doan, T. V.; Bostrom, N. W.; Burnham, A. K.; Kleinberg, R. L.; Pomerantz, A. E.; Allix, P. Green River oil shale pyrolysis: Semi-open conditions. *Energy Fuels* **2013**, *27*, 7447−6459.
(9) Speight, J. G. The application of spectroscopic techniques to the structural analysis of coal and petroleum. *Appl. Spectrosc. Rev.* **1972**, *5*, 211−263.
(10) Rouxhet, P. G.; Robin, P. L.; Nicaise, G., Characterization of kerogens and of their evolution by infrared spectroscopy. In *Kerogen—Insoluble Organic Matter from Sedimentary Rocks*; Durand, B., Ed.; Editions Technip: Paris, 1980.
(11) Painter, P. C.; Snyder, R. W.; Starsinic, M.; Coleman, M. M.; Kuehn, D. W.; Davis, A. Concerning the application of FTIR to the study of coal: A critical assessment of band assignments and the application of spectral analysis programs. *Appl. Spectrosc.* **1981**, *35*, 475−485.
(12) Wang, S.-H.; Griffiths, P. R. Resolution enhancement of diffuse reflectance i.r. spectra of coals by Fourier self-deconvolution. 1. C—H stretching and bending modes. *Fuel* **1985**, *64*, 229−236.
(13) Ganz, H.; Kalkreuth, W. Application of infrared spectroscopy to the classification of kerogen-types and the evaluation of source rock and oil shale potentials. *Fuel* **1987**, *66*, 708−711.
(14) Christy, A. A.; Kvalheim, O. M.; Oygard, K.; Dahl, B.; Karstang, T. V. Maturity of kerogen and asphaltenes determine by partial-least-squares (PLS) calibration and target projection of diffuse reflectance Fourier transformed infrared spectra. *Org. Geochem.* **1991**, *17*, 63−74.
(15) Lin, R.; Ritz, G. P. Studying individual macerals using i.r. microspectroscopy, and implications on oil versus gas/condensate proneness and "low-rank" generation. *Org. Geochem.* **1993**, *20*, 697−706.
(16) Iglesias, M.; Jiménez, A.; Laggoun-Défarge, F.; Suárez-Ruiz, I. FTIR study of pure vitrains and associated coals. *Energy Fuels* **1995**, *9*, 458−466.
(17) Ibarra, J. V.; Munoz, E.; Moliner, R. FTIR study of the evolution of coal structure during the coalification process. *Org. Geochem.* **1996**, *24*, 725−735.
(18) Guo, Y.; Bustin, R. M. Micro-FTIR spectroscopy of liptinite macerals in coal. *Int. J. Coal Geol.* **1998**, *36*, 259−275.
(19) Lis, G. P.; Mastalerz, M.; Schimmelmann, A.; Lewan, M. D.; Stankiewicz, B. A. FTIR absorption indices for thermal maturity in comparison with vitrinite reflectance R_o in type-II kerogen from Devonian black shales. *Org. Geochem.* **2005**, *36*, 1533−1552.
(20) Petersen, H. I.; Rosenberg, P.; Nytoft, H. P. Oxygen groups in coals and alginite-rich kerogen revisited. *Int. J. Coal Geol.* **2008**, *74*, 93−113.
(21) Chen, Y.; Mastalerz, M.; Schimmelmann, A. Characterization of chemical functional groups in macerals across different coal ranks via micro-FTIR spectroscopy. *Int. J. Coal Geol.* **2012**, *104*, 22−33.
(22) Tissot, B.; Deroo, G.; Hood, A. Geochemical study of the Uinta Basin: Formation of petroleum from the Green River formation. *Geochim. Cosmochim. Acta* **1978**, *42*, 1469−1485.
(23) Miknis, F. P.; Turner, T. F. The Bitumen intermediate in isothermal and nonisothermal decomposition of oil shales. In *Composition, Geochemistry and Conversion of Oil Shales*; Snape, C., Ed.; NATO ASI Series; Springer-Verlag: Berlin, **1995**; Vol. *455*.
(24) Borrego, A. G.; Blanco, C. G.; Prado, J. G.; Díaz, C.; Guillén, M. D. ^{1}H NMR and FTIR spectroscopic studies of bitumen and shale oil from selected Spanish oil shales. *Energy Fuels* **1996**, *10*, 77−84.
(25) Feng, Y.; Le Doan, T. V.; Pomerantz, A. E. The chemical composition of bitumen in pyrolyzed Green River oil Shale: Characterization by ^{13}C NMR Spectroscopy. *Energy Fuels* **2013**, *27*, 7314−7323.
(26) Johnson, R. C. Early Cenozoic history of the Uinta and Piceance Creek basins, Utah and Colorado, with special reference to the development of Eocene Lake Uinta. In *Cenozoic Paleogeography of the West-Central United States*; Rocky Mountain Section, Society of Economic Paleontologists and Mineralogists: Denver, CO, **1985**.
(27) Sweeney, J. J.; Burnham, A. K. Evaluation of a simple model of vitrinite reflectance based on chemical kinetics. *AAPG Bull.* **1990**, *74*, 1559−1570.
(28) Sweeney, J. J.; Burnham, A. K. Errata for Sweeney and Burnham (1990). *AAPG Bull.* **1991**, *75*, 848.
(29) Durand, B.; Nicaise, G. Procedures for kerogen isolation. In *Kerogen-Insoluble Organic Matter from Sedimentary Rocks*; Durand, B., Ed.; Editions Technip: Paris, 1980.
(30) Duyckaerts, G. The infra-red analysis of solid substances. *Analyst* **1959**, *84*, 201−214.
(31) Barth, T.; Seim, M.; Christy, A. A.; Kvalheim, O. M. Maturity trends in asphaltenes from pyrolyzed source rocks and natural coals-multivariate modelling of diffuse reflectance Fourier-transform infrared spectra. *Org. Geochem.* **1995**, *23*, 139−158.
(32) Christy, A. A.; Hopland, A. L.; Barth, T.; Kvalheim, O. M. Quantitative determination of thermal maturity in sedimentary organic matter by diffuse reflectance infrared spectroscopy of asphaltenes. *Org. Geochem.* **1989**, *14*, 77−81.
(33) Miller, F. A.; Wilkins, C. H. Infrared spectra and characteristic frequencies of inorganic ions. *Anal. Chem.* **1952**, *24*, 1253−1294.
(34) Tissot, B.; Durand, B.; Espitalié, J.; Combaz, A. Influence of the nature and diagenesis of organic matter in formation of petroleum. *AAPG Bull.* **1974**, *58*, 499−506.
(35) Durand, B.; Espitalié, J. Geochemical studies on the organic matter from the Douala Basin (Cameroon)—II. Evolution of kerogen. *Geochim. Cosmochim. Acta* **1976**, *40*, 801−808.
(36) Maddams, W. F. The scope and limitations of curve fitting. *Appl. Spectrosc.* **1980**, *34*, 245−267.
(37) Meier, R. J. On art and science in curve-fitting vibrational spectra. *Vib. Spectrosc.* **2005**, *39*, 266−269.
(38) Fuller, M. P.; Hamadeh, I. M.; Griffiths, P. R.; Lowenhaupt, D. E. Diffuse reflectance infrared spectrometry of powdered coals. *Fuel* **1982**, *61*, 529−536.
(39) Miknis, F. P.; Turner, T. F.; Berdan, G. L.; Conn, P. L. Formation of soluble products from thermal decomposition of Colorado and Kentucky oil shale. *Energy Fuels* **1987**, *1*, 477−483.
(40) Salmon, E.; Behar, F.; Hatcher, P. G. Molecular characterization of Type I kerogen from the Green River Formation using advanced NMR techniques in combination with electrospray ionization/ultrahigh resolution mass spectrometry. *Org. Geochem.* **2013**, *42*, 301−315.
(41) Pomerantz, A. E.; Bake, K. D.; Craddock, P. R.; Kurzenhauser, K. W.; Kodalen, B. G.; Mitra-Kirtley, S.; Bolin, T. B. Sulfur speciation

DOI: 10.1021/ef5027532
Energy Fuels 2015, 29, 2197−2210

in kerogen and bitumen from gas and oil shales. *Org. Geochem.* **2014**, *68*, 5−12.
(42) Rouxhet, P. G.; Robin, P. L. Infrared study of the evolution of kerogens of different origins during catagenesis and pyrolysis. *Fuel* **1978**, *57*, 533−540.
(43) Burnham, A. K.; Clarkson, J. E.; Singleton, M. F.; Wong, C. M.; Crawford, R. W. Biological markers from Green River kerogen decomposition. *Geochim. Cosmochim. Acta* **1982**, *46*, 1243−1261.
(44) Huss, E. B.; Burnham, A. K. Gas evolution during pyrolysis of various Colorado oil shales. *Fuel* **1982**, *61*, 1188−1196.
(45) Sanderson, R. T. *Chemical Bonds and Bond Energy*; Academic Press: New York, NY, 1976.
(46) Luo, Y.-R. *Comprehensive Handbook of Chemical Bond Energies*. CRC Press: Boca Raton, FL, 2007.
(47) Miknis, F. P.; Szeverenyi, N. M.; Maciel, G. E. Characterization of the residual carbon in retorted oil shale by solid-state ^{13}C n.m.r. *Fuel* **1982**, *61*, 341−345.
(48) Cao, X.; Birdwell, J. E.; Chappell, M. A.; Li, Y.; Pignatello, J. J.; Mao, J. Characterization of oil shale, isolated kerogen, and postpyrolysis residues using advanced ^{13}C nuclear magnetic resonance spectroscopy. *AAPG Bull.* **2013**, *97*, 421−436.
(49) Kelemen, S. R.; Afeworki, M.; Gorbaty, M. L.; Sansone, M.; Kwiatek, P. J.; Walters, C. C.; Freund, H.; Siskin, M.; Bence, A. E.; Curry, D. J.; Solum, M.; Pugmire, R. J.; Vandenbroucke, M.; Leblond, M.; Behar, F. Direct characterization of kerogen by X-ray and solid-state ^{13}C nuclear magnetic resonance methods. *Energy Fuels* **2007**, *21*, 1548−1561.
(50) Mao, J.; Fang, X.; Lan, Y.; Schimmelmann, A.; Mastalerz, M.; Xu, L.; Schmidt-Rohr, K. Chemical and nanometer-scale structure of kerogen and its change during thermal maturation investigated by advanced solid-state ^{13}C NMR spectroscopy. *Geochim. Cosmochim. Acta* **2010**, *74*, 2110−2127.
(51) Coburn, T. T.; Campbell, J. H. *Oil Shale Retorting: Part 2 Variation in Product Oil Chemistry During Retorting of an Oil Shale Rock*; UCRL-52256 Part 2; Lawrence Livermore Laboratory: Livermore, CA, 1977.

DOI: 10.1021/ef5027532
Energy Fuels 2015, 29, 2197−2210